Structural, Magnetic, and Magnetoresistive Properties of Electrodeposited Ni 5 Zn 21 Alloy Nanowires

ARTICLE *in* THE JOURNAL OF PHYSICAL CHEMISTRY B · NOVEMBER 2006

Impact Factor: 3.3 · DOI: 10.1021/jp062784u · Source: PubMed

Structural, Magnetic, and Magnetoresistive Properties of Electrodeposited Ni_5Zn_{21} Alloy Nanowires

Lifeng Liu,[†,‡] Huanfang Tian,[†,‡] Sishen Xie,*[,†] Weiya Zhou,[†] Shicheng Mu,[§] Li Song,[†,‡] Dongfang Liu,[†,‡] Shudong Luo,[†,‡] Zengxing Zhang,[†,‡] Yanjuan Xiang,[†,‡] Xiaowei Zhao,[†,‡] Wenjun Ma,[†,‡] Jun Shen,[†,‡] Jianqi Li,[†] Chaoying Wang,[†] and Gang Wang[†]

Beijing National Laboratory for Condensed Matter Physics and Institute of Physics, Chinese Academy of Sciences, Beijing 100080, People's Republic of China, The Graduate University, Chinese Academy of Sciences, Beijing 100049, People's Republic of China, and Nanotechnology Industrialization Base of China, TEDA, Tianjin 300457, People's Republic of China

Received: May 7, 2006; In Final Form: August 9, 2006

Ni_5Zn_{21} alloy nanowires were fabricated through template-assisted electrochemical deposition method. The morphology and microstructures of as-deposited nanowires were determined by field-emission scanning electron microscope (FE-SEM), X-ray diffraction (XRD), high-resolution transmission electron microscope (HRTEM), electron diffraction (ED), and electron probe microanalysis (EPMA). The accurate composition was measured via induced coupling plasma atomic emission spectroscopy. SEM results show that Ni_5Zn_{21} nanowires are deposited in most of the nanopores of the template, and they are continuous and dense throughout the whole length. The XRD result demonstrates that the nanowires are mainly composed of a cubic γ phase Ni_5Zn_{21} alloy, but there also exists a trace of Zn-rich η phase. HRTEM and ED reveal that the alloy nanowires are polycrystalline with the crystallite size of several tens of nanometers. EPMA of a single nanowire illustrates that there exist Ni-rich microzones in as-deposited nanowires. Subsequent magnetic measurements of the array also confirmed the existence of them. In addition, it can be further inferred that the shape of Ni-rich microzones is probably barlike or disklike, from the anisotropy of zero field cooling/field cooling (ZFC/FC) curves as well as the vortex magnetization behavior of the Ni_5Zn_{21} nanowire array. The low-temperature magnetoresistance of the Ni_5Zn_{21} nanowire array was also measured. Giant magnetoresistance instead of anisotropic magnetoresistance is suggested to be responsible for contributing to the magnetoresistance.

1. Introduction

In recent years, magnetic nanowires have attracted more and more attention because of their significance in both fundamental research and practical applications.[1−3] However, current studies mostly concentrate on ferromagnetic metallic nanowires and alloy nanowires consisted of two or three kinds of pure magnetic metals. The reports on ferromagnetic−nonmagnetic (FM-NM) heterogeneous alloy nanowires are limited.[4−12] For FM-NM alloy, the introduction of magnetic element into nonmagnetic matrix usually has a significant impact on the structure, magnetism, and electrical transport of the alloy and can cause some interesting properties such as mixed magnetism, giant magnetoresistance (GMR) effect, etc.[13,14] With the rapid development of nanoscience and technology, investigating the preparation, structures, and properties of FM-NM alloy nanowires is stimulating much more interests. However, the fabrication of alloy nanowires is usually difficult via common solution-based syntheses or other traditional physical and chemical vapor deposition approaches. Template synthesis together with electrochemical deposition (ECD) is now considered as one of the most suitable methods to obtain alloy nanowires. Not only can the size of deposited nanowires be easily controlled by choosing template with different pore diameters (may vary from several nanometers to several hundreds of nanometers), but also the composition of nanowires can be modulated via changing ECD parameters (the electrolytes, the deposition potential, and current density, etc.).

Most present studies on FM-NM alloy nanowires are concentrated on Cu-based, Ag-based, and Pt-based systems,[4−12] that is, using Cu, Ag, and Pt as nonmagnetic matrixes. The reports on Zn-based FM-NM alloy nanowires are very few. Recently, Jia and co-workers reported the synthesis and structures of Ni_5Zn_{21} nanowires fabricated by electrodeposition in porous anodic alumina (PAA) template.[15] Independently, we also successfully prepared large-diameter Ni_xZn_{1-x} alloy nanowires with controllable composition.[16] Furthermore, we studied the relation between composition and structures of as-deposited nanowires and found that the structures of Ni_xZn_{1-x} nanowires could vary from a single hexagonal η phase to the coexistence of η phase and cubic γ phase, with the increase of nickel content. Up to now, however, the detailed structural characters as well as magnetic and transport properties of Ni_xZn_{1-x} nanowires have not been reported.

In this article, we report the synthesis of Ni_5Zn_{21} nanowires of 60 nm diameter and lengths of several tens of micrometerss, using our homemade PAA templates. Detailed structural investigations show that there exist Zn-rich (η phase) and Ni-rich microzones in the as-deposited alloy nanowires, which were introduced by the nonequilibrium electrodeposition process. The magnetic measurements reveal that the as-deposited Ni_5Zn_{21}

* To whom correspondence should be addressed. Telephone: +86-10-82649081. Fax: +86-10-82640215. E-mail: ssxie@aphy.iphy.ac.cn.
† Beijing National Laboratory for Condensed Matter Physics and Institute of Physics, Chinese Academy of Science.
‡ The Graduate University, Chinese Academy of Science.
§ Nanotechnology Industrialization Base of China.

10.1021/jp062784u CCC: $33.50
Published on Web 09/06/2006

nanowires are superparamagnetic and exhibit interesting vortex magnetization with the increasing temperature. Such vortex magnetization behavior has not been reported in other magnetic nanowires so far. The low-temperature magnetoresistance of Ni_5Zn_{21} nanowire array was also measured, and a GMR character is revealed.

2. Experimental Section

2.1. Fabrication of PAA Template and Ni_5Zn_{21} Nanowires. The PAA templates used in our experiments were prepared by two-step anodization method developed by Masuda and Sotah.[17] Briefly, a piece of high-purity aluminum (99.999%) with the dimensions of 5 cm × 2 cm × 0.5 mm was first anodized in 0.3 M oxalic acid at 1×c1ãC under 40 V voltage; then the aluminum foil with a layer of porous alumina was submerged in the mixed solution of 5 wt % H_3PO_4 and 1.8 wt % CrO_3 at 60 °C for several hours, to remove the oxidized layer. The second anodization was performed for 15 h under the condition identical with the first anodization. After the second anodization, the oxidized layer was detached by soaking the aluminum foil into saturated $HgCl_2$ solution. Then the separated PAA membrane was put in 5 wt % H_3PO_4 for 90 min at 30 °C to etch away the barrier layer and widen the pores. Thus, the through-hole PAA template was obtained. The pore diameter is about 60 ± 5 nm on average, and the film thickness is about 40 μm.

Before performing ECD experiment, a layer of Au was sputtered on one side of the through-hole PAA template through an ion sputtering system (Hitachi E1030, 20 mA, 1000 s). The ECD was carried out in a traditional two-electrodes cell at 25 °C. A piece of high-purity Ni plate (99.99%) and another piece of Zn plate (99.99%) were chosen as the anodes together, and the Au-coated PAA was used as working electrode. The electrolyte consisted of 100 g/L $ZnCl_2$, 80 g/L $NiCl_2$, and 220 g/L NH_4Cl with 318 MΩ deionized water as solvent. All the chemicals mentioned above are analytical reagents. The deposition was conducted under galvanostatic mode with the current density of 30 mA/cm^2. The deposition time is set as 80 min.

2.2. Characterization and Measurements. The morphology and composition of as-deposited nanowires were characterized by a field-emission scanning electron microscope (FE-SEM, Hitachi S-5200) equipped with energy disperse X-ray spectrum (EDX, Thermoelectron). Induced coupling plasma atomic emission spectrometer (ICP-AES, Thermoelectron, IRIS Intrepid II) was used to determine the atomic ratio of Ni and Zn accurately. X-ray diffraction (XRD) was performed at Bruker diffractometer (D8 Advance) with Cu Kα radiation (λ = 1.540 60 Å). High-resolution transmission electron microscope (HRTEM) and electron diffraction (ED) were taken at an FE-TEM (JEOL JEM-2010FEF) working at 200 keV. Electron probe microanalysis (EPMA) on a single nanowire was conducted at an FE-TEM (Tecnai F20) with a nanosized electron beam (~5 nm). For TEM observation, the template filled with as-deposited nanowires was immersed into 2 M NaOH solution for 10−15 min at 25 °C. It was found that such immersion time just could remove alumina completely, and longer immersion would make the as-deposited nanowires dissolve as well.[15] Then, the released nanowires were washed carefully with distilled water for several times and were subjected to ultrasonic treatment for 1 min. A drop of suspension was dripped on carbon-coated copper grid for TEM study, and also some drops were dripped on silicon substrate for SEM observation.

The magnetic measurements of alloy nanowire array were conducted at a superconducting quantum interference device (SQUID, MPMS-7, Quantum Design) within the temperature range of 5−300 K. Zero-field cooling (ZFC) and field cooling (FC) magnetization−temperature ($M-T$) curves, and magnetic hysteresis loops (M−H) at different temperatures with magnetic field parallel and perpendicular to the long axes of nanowires (abbreviated as parallel configuration and perpendicular configuration) were measured, respectively. The magnetoresistance measurement of the nanowire array was performed at commercialized physical property measuring system (PPMS, Quantum Design) at 5 K with a modified four-electrodes configuration.

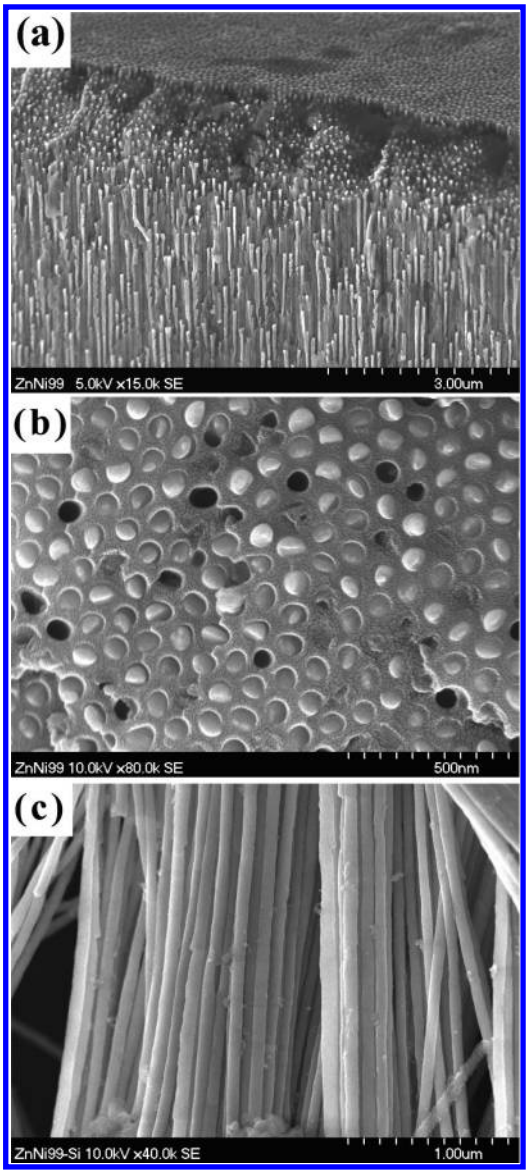

Figure 1. (a) Overview and (b) top view of Ni_5Zn_{21} nanowire array embedded in the PAA template; (c) Ni_5Zn_{21} nanowires released from the PAA template.

3. Results and Discussions

3.1. Morphology and Structures of Ni_5Zn_{21} Alloy Nanowires. Figure 1a shows an overview of the as-deposited nanowires embedded in the PAA template. It is clear that a large area of nanopores was filled with the deposited nanowires. These nanowires are highly parallel to each other and normal to the surface of the template. Shown in Figure 1b is the top view of the array, which illustrates that the filling degree is very high, nearly amounting to 90%. It also shows that the as-deposited nanowires filled the nanopores closely so that they replicated

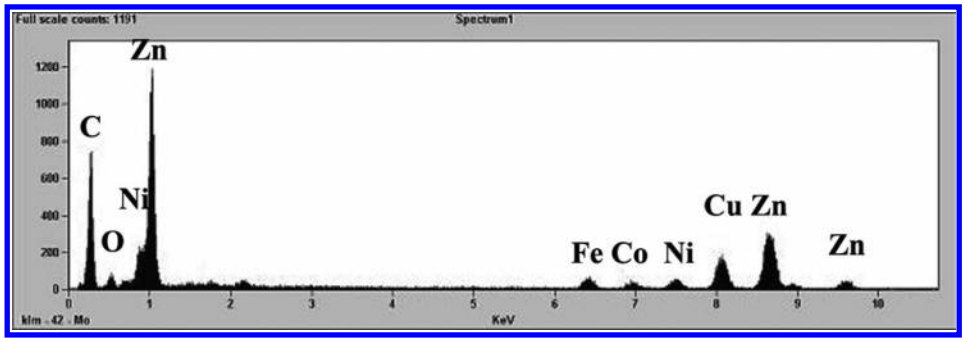

Figure 2. EDX spectrum of as-deposited Ni_5Zn_{21} nanowires.

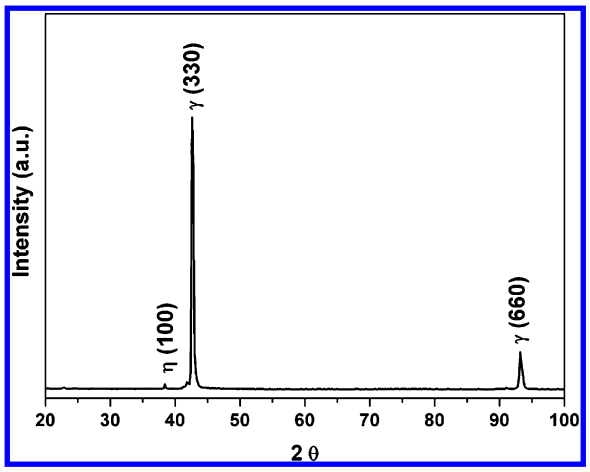

Figure 3. XRD pattern of Ni_5Zn_{21} nanowire array embedded in the PAA template.

the pore diameter strictly. Figure 1c is a magnified cross-sectional image of the nanowire array after removing the alumina template. It can be seen that these nanowires are continuous, dense, and uniform along the axial direction. Their diameters are about 60 ± 5 nm, consistent with the diameters of the nanopores.

To confirm the composition of as-prepared nanowires, the EDX analysis was performed at SEM working at scanning transmission electron microscope (STEM) mode. Figure 2 shows a typical EDX spectrum of as-deposited nanowires. It clearly confirms that the nanowires consist of nickel and zinc, and other elements shown in this spectrum come from the carbon-coated copper grid. Since the EDX analysis is semiquantitative, ICP-AES measurement was carried out for obtaining the accurate atomic ratio of Ni and Zn. The ICP-AES result shows that the atomic ratio of Ni and Zn is very close to 5:21. Therefore, the as-deposited alloy nanowires can be confirmed as Ni_5Zn_{21} nanowires.

Figure 3 gives a typical XRD pattern of Ni_5Zn_{21} alloy nanowires embedded in the PAA template. There only exist three peaks in a wide angular range: the weakest peak centered at 38.4°, the strongest peak centered at 43.1°, and a relatively weak peak centered at 93.5°. According to previous studies on nickel−zinc electrodeposits,[18,19] there are two structures in as-deposited nickel−zinc alloy with the variation of nickel, hcp η phase with a distorted lattice and bcc γ phase based on 5:21 stoichiometric nickel−zinc alloy (JCPDF No. 06-653). In our XRD pattern, the three peaks can be indexed as η (100), γ (330), and γ (660), respectively. Especially, it is found that the high-intensity γ (330) and γ (660) peaks agree well with Ni_5Zn_{21} standard diffractions (JCPDF No. 06-653), confirming the Ni_5Zn_{21} phase actually dominates in the as-deposited nanowires. This is consistent with the ICP-AES result. According to the electrodeposited nickel−zinc alloy phase diagram suggested by Bruet-Hotellza et al.,[19] when the Ni content is beyond 14.1 at. %, only a single phase, the γ phase, could be observed. Our result basically agrees with the proposed electrodeposited nickel−zinc alloy phase diagram. The exact reason of the existence of a trace of η phase is not very clear up to now. However, it is presumed that, on one hand, it is related to the preferred deposition of zinc at the initial stage of electrodeposition;[16] on the other hand, the confinement of the nanopores may enhance the nonequilibrium deposition process to some extent so as to lead to the occurrence of a trace of the η phase. Another noteworthy point in the XRD pattern is that there are only the peaks arisen from the diffractions of γ {110} lattice planes family, illustrating that these nanowires preferably orientated along the bcc ⟨110⟩ direction.

Compared with the γ phase nickel−zinc solid solution, the η phase represents Zn-rich phase actually. Therefore, for the stoichiometric Ni_5Zn_{21} alloy, the existence of the Zn-rich η phase means that there should also exist a Ni-rich phase. In fact, the EPMA of a single nanowire as well as the magnetic and GMR characters that will be mentioned below indeed confirm the existence of Ni-rich microzones in as-deposited Ni_5Zn_{21} nanowires (at least some of the nickel in the alloy is in pure Ni phase). The absence of nickel reflections in the XRD spectrum is probably related to the relatively low content and to the small size of Ni-rich microzones.

For further structural characterizations, we carried out TEM, HRTEM, and ED studies. Figure 4a gives a low-magnification TEM picture. It shows that these Ni_5Zn_{21} nanowires are continuous, and their length is up to several tens of micrometers. A magnified TEM image is given in Figure 4b, further confirming that these nanowires are dense and uniform in diameter, instead of the aggregation of granulae. However, a close view denoted in the inset of Figure 4b shows that the surface of the nanowire, in fact, is not very smooth. It is believed that the roughness is the replica of the unsmoothness of the inner wall of the nanopores. Electron diffraction was used to determine the crystallization of as-deposited Ni_5Zn_{21} nanowires. A typical ED pattern taken from the selected circle area denoted in Figure 5a is given in Figure 5b. This pattern corresponds to the diffractions of the ⟨111⟩ zone axis of the bcc γ phase nickel−zinc alloy. It is clear that the selected area is well crystallized, and the crystalline domain is about several tens of nanometers. In addition, it is found that the diffraction spots of {330} and {660} plane families are brighter that other spots. This is a general characteristic for a Hume−Rothery alloy, in which the Jones zone of the γ phase is enclosed with the family of the {330} and {411} crystal planes so that it will give rise to the strongest X-ray diffraction for these crystal planes.[20] Such an

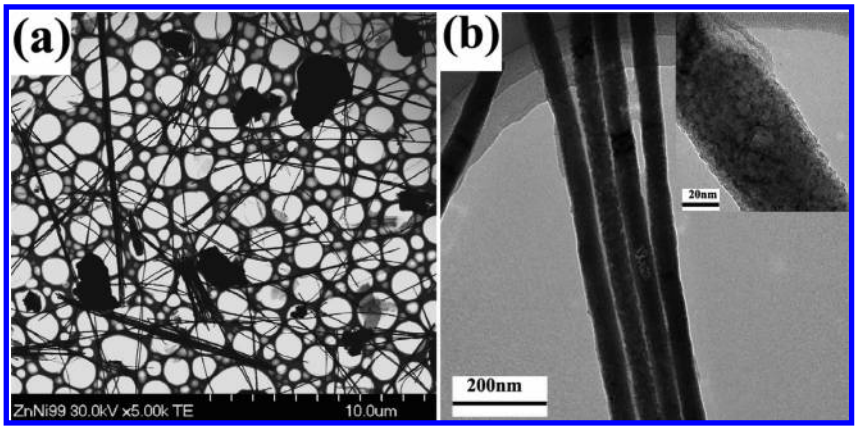

Figure 4. TEM images of as-deposited Ni_5Zn_{21} nanowires: (a) low magnification; (b) high magnification. Inset: close view of the nanowire surface.

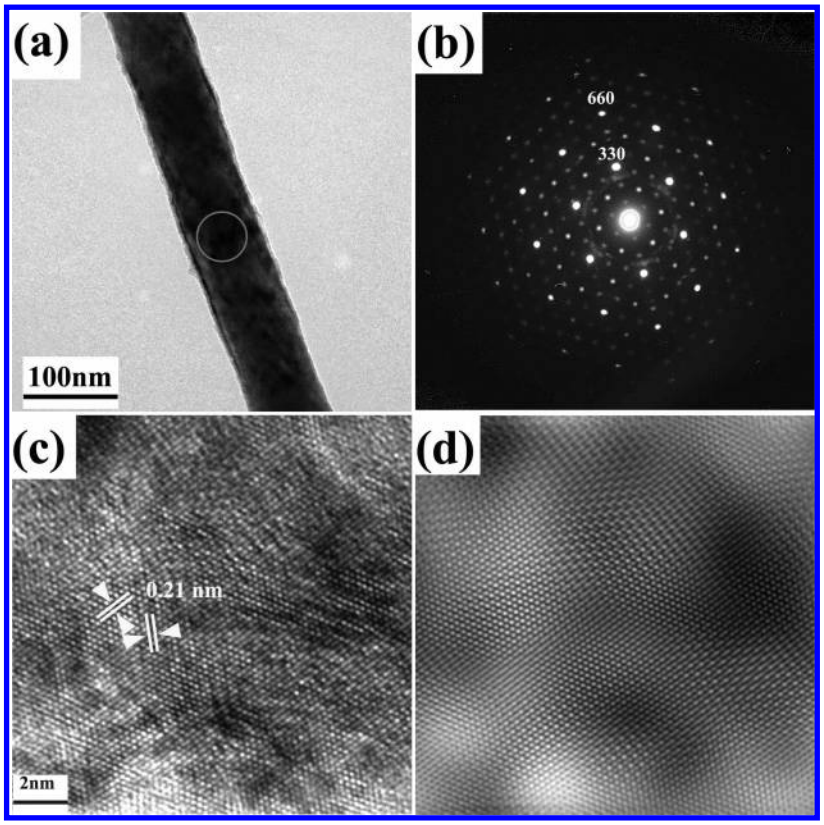

Figure 5. (a) TEM image of a single Ni_5Zn_{21} nanowire; (b) ED pattern taken from the circle area shown in a; (c) HRTEM image of the circle area shown in a; (d) FFT image of c.

ED result is also in accord with the XRD pattern mentioned above, which shows that (330) and (660) directions have higher diffraction intensity. The HRTEM image of the corresponding selected area is given in Figure 5c. It shows that the lattice exhibits a well-defined hexagonal arrangement, consistent with the ED pattern. The spacing of the hexagonal lattice is about 0.21 nm, corresponding to that of γ {330} lattice planes (0.2109 nm, JCPDF 06-0653). Figure 5d gives a fast Fourier transform (FFT) image of Figure 5c. It can be seen that there exist relatively large lattice distortions in this crystalline area. In addition to the influence of surface roughness of nanowires, these distortions may be attributed to the stress arisen from the nonequilibrium electrodeposition and the confinement effect of the nanopores, which would result in defects and dislocations in the nanowires.

We also made an attempt to search the Ni-rich microzones we expected above through HRTEM and diffraction contrast imaging, but we failed to do this, unfortunately. This mainly lies in the fact that the size of such microzones is very small and some of them have dispersed or embedded in the lattices of the alloy; on the other hand, the atomic order of nickel and zinc is very close so that it is difficult to distinguish them from a conventional diffraction contrast image.[21] Thus, to detect the existence of Ni-rich microzones, EPMA, which can give elemental profiles when performing a line scan, perhaps is a suitable tool. If the Ni-rich microzones exist, they can be reflected by the variation of composition. The probe is the focused nanosized electron beam in FE-TEM, with the diameter of ~5 nm. Using this microprobe, a line scan was carried out along both radial and axial directions of a single nanowire, just like the pictures shown in Figure 6a,b. The corresponding elemental profiles are shown in Figure 6c,d, respectively. In Figure 6c, it can be seen that both Ni and Zn begin to increase from the starting point of the scan, reach the summit, and then

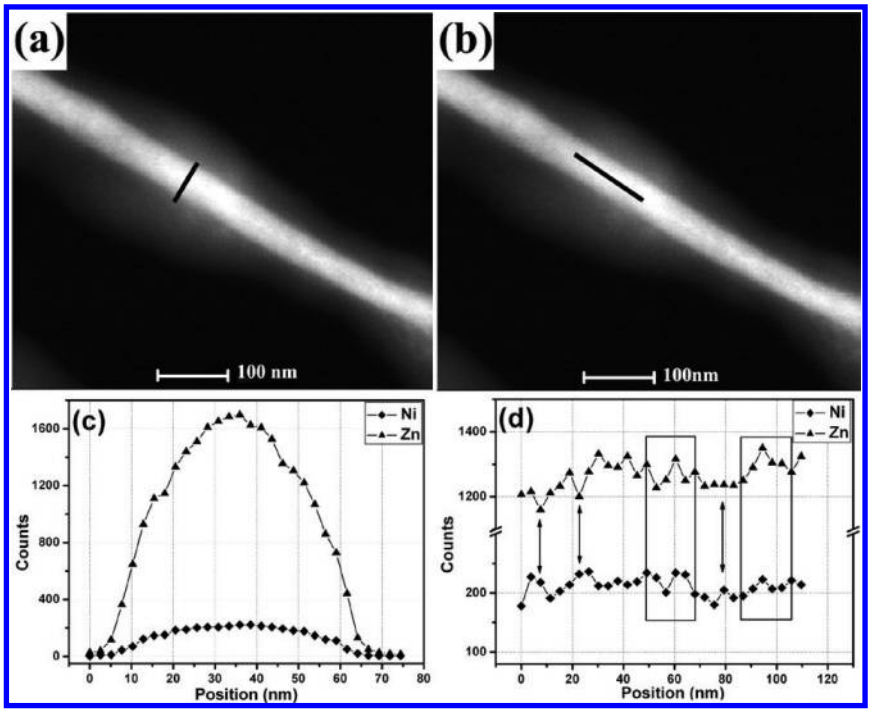

Figure 6. Scanning transmission electron microscopic (STEM) images and electron probe microanalyses of a single Ni_5Zn_{21} nanowire: (a, b) STEM images of a single Ni_5Zn_{21} nanowire; (c) elemental profiles when line-scanning in the radial direction; (d) elemental profiles when line-scanning in the axial direction.

decrease to original concentrations. Such concentration variations are mainly due to the cylinder shape of the nanowire; moreover, the symmetry of the profiles demonstrates that both Ni and Zn distribute uniformly along the radial direction. In Figure 6b, a length of 110 nm along the axial direction was chosen to perform the line scan. The distance between neighbor points is about 4 nm, slightly smaller than the diameter of the electron beam, so that the beam can cover all areas along the scan line. It is evident from Figure 6d that both Ni and Zn fluctuate along the nanowire axis. In addition, the fluctuations can be classified as two: one is the Ni peak together with the Zn valley at the same position, which is shown by arrows. For the stoichiometric alloy, such fluctuations mean the nonuniformity of composition, and are suggestive of the existence of Ni-rich microzones along the axial direction. Considering the superposition of the electron beam between neighbor detection points, it is estimated that the size of Ni-rich microzones is about 3−4 nm. Another kind of fluctuation is that both Ni and Zn increase or decrease simultaneously, just like what is denoted with squares. Such fluctuations are probably not arisen from the nonuniformity of composition, but from the unsmoothness of the surface of the studied nanowire. Therefore, we can conclude that although HRTEM and diffraction contrast image fail to observe the Ni-rich microzones, the EPMA result indeed supports their existence.

3.2. Magnetic and Magnetoresistive Properties of Ni_5Zn_{21} Nanowire Array. The magnetic properties of the as-deposited Ni_5Zn_{21} nanowire array were measured with parallel and perpendicular configurations, respectively.

Figure 7a shows the zero field cooling (ZFC) and field cooling (FC) magnetization curves of Ni_5Zn_{21} nanowire array as a function of temperature under these two measurement configurations. For ZFC measurement, the sample was cooled to 5 K in zero field and then measured up to 300 K in a field of 500 Oe, while the FC measurement was made by cooling the sample from 300 to 5 K in the same field. It clearly shows that there is a furcation between ZFC and FC curves at a certain temperature (denoted as T_{diff} herein), which is one of the characteristic features of a superparamagnetic system.[22] This fact further confirms our previous results that there exist some magnetic Ni-rich microzones in the nanowires. Moreover, it is found that the blocking temperatures, T_B, defined as the temperature with maximum magnetization in the ZFC curve, of both parallel and perpendicular configurations have a slight difference and are both lower than the furcation temperature, T_{diff}. Such behavior usually indicates a certain size distribution of magnetic microzones. A fraction of the largest magnetic microzones already freezes at T_{diff}, and the majority fraction of the magnetic microzones is being blocked at T_B. Despite the similarity of the ZFC/FC curves measured in parallel and perpendicular configurations, they still have some differences. First, the magnetization of the parallel configuration is slightly higher than that of the perpendicular configuration. This may be due to the fact that in perpendicular measurement configuration the nonmagnetic alumina walls of nanopores probably interrupt the interactions among some of the magnetic microzones so as to give rise to relatively low magnetization. The second difference is that the T_{diff} of the perpendicular configuration is higher than that of the parallel configuration. The true reason resulted in this difference is not clearly known now. However, as mentioned above, T_{diff} is related to the size distribution of magnetic microzones, and it will increase with microzone size.[22] Therefore, we assumed that the shape of the Ni-rich microzones in the nanowires is probably platelike and most plates are normal to the long axes of the nanowires. Such assumption is in accord with the EPMA result, which shows the Ni-rich microzones are only detected in the axial direction. This is also intelligible because the nanowires are deposited along the long axes direction, so it is more preferable to form platelike Ni-rich microzones. Thus, the shape anisotropy of magnetic microzones gives rise to the anisotropy of T_{diff}.

On the other hand, it is also noted that, unlike other immiscible alloys such as the widely studied CoCu,[5,13,23] the difference of magnetization between ZFC and FC data at low

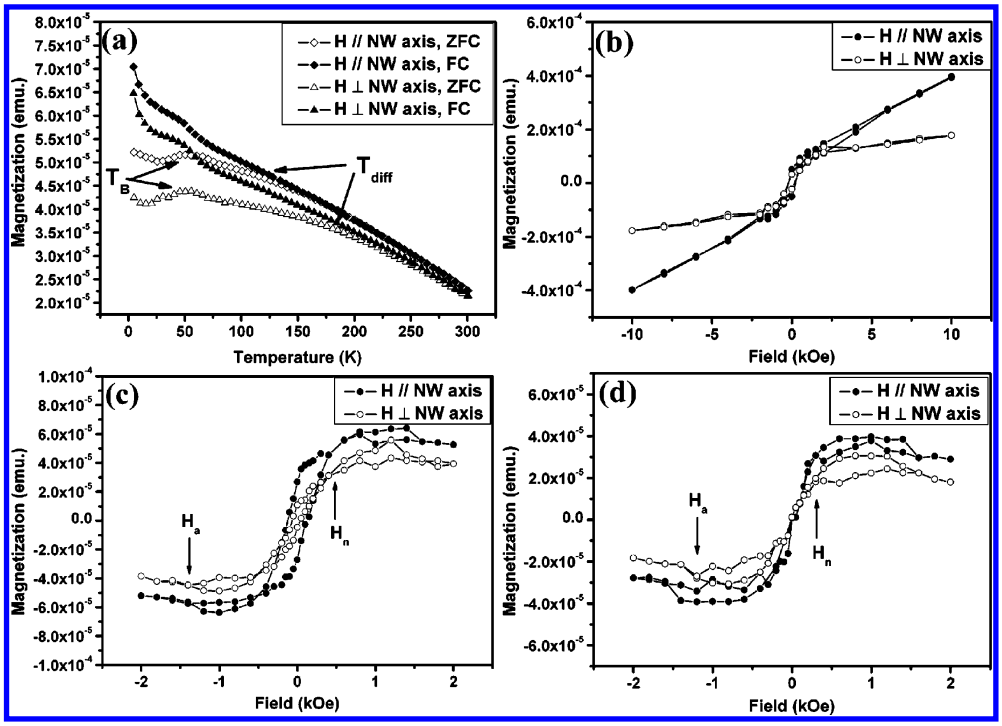

Figure 7. (a) ZFC/FC magnetization curves of as-deposited Ni_5Zn_{21} nanowire array embedded in PAA template; (b) magnetic hysteresis loops measured at 5 K; (c) magnetic hysteresis loops measured at 100 K; (d) magnetic hysteresis loops measured at 250 K.

temperature is relatively small. This reflects the number of Ni-rich microzones is not abundant. The small amount of Ni-rich microzones lies in the fact that nickel and zinc are miscible and more easily alloyed, while cobalt and copper are immiscible, so that cobalt is prone to precipitate from the metastable alloy. It is also found that the ZFC/FC curves in our case are more similar to those of the FeZr alloy,[24] which consists of small Fe clusters embedded in a nonmagnetic alloy matrix.

The magnetic hysteresis loops of the Ni_5Zn_{21} alloy nanowire array were also measured at different temperatures. Parts b−d of Figure 7 show the results measured at 5, 100, and 250 K. At 5 K, hysteresis occurs in both parallel and perpendicular configurations, revealing a softly ferromagnetic behavior. The coercivities of these two configurations are similar, both about 290 Oe. When the temperature increases beyond 100 K, it is found that the relatively low applied field can make the magnetization saturated. If the applied field is higher than 2 kOe, the diamagnetic contributions of the PAA template will be comparable with the magnetization of Ni_5Zn_{21} nanowires so that the total magnetization reduces rapidly instead of tending to be saturated. Hence, the range of the applied field is only limited within ±2 kOe at 100 and 250 K. At 100 K, it is found that the ferromagnetism still remains, but the coercivities show slight anisotropy. The coercivity of parallel configuration is about 125 Oe, larger than that of the perpendicular configuration, 55 Oe. Moreover, the hysteresis loops begin to exhibit vortex magnetic characters. When the temperature reaches 250 K, above T_{diff}, the remanent magnetization turns to be zero at zero field and the hysteresis disappears, showing a paramagnetic behavior. What is more, the vortex magnetization seems to be more obvious.

Now we examine the origin of the magnetism in Ni_5Zn_{21} nanowires further. It is well-known that the ferromagnetic saturation moment of nickel is 0.6 μ_B (μ_B is the Bohr magneton) at absolute zero.[25] Such a value can be understood from the following:[26] the outer 10 electrons of nickel are divided between the 3d and the 4s bands in such a way that on average there is 0.6 electron per atom in the 4s band and 0.6 electron per atom missing from the 3d band. The ferromagnetic moment below the Curie point and the paramagnetic moment above it are due to the holes in the 3d band. When nickel is alloyed with zinc, the 4s electrons supplied by zinc will tend to fall into the holes in the 3d band of the alloy until the 3d band is full. This will occur at 30% zinc according to the previous studies.[27] Hence, for as-prepared Ni_5Zn_{21} alloy nanowires, it should have shown no ferromagnetism because the holes of the 3d band of the alloy have been filled and the ferromagnetic moments tend to be zero. However, the magnetic hysteresis loops demonstrate that soft ferromagnetism exists at least at 100 K. This further illustrates the existence of Ni-rich microzones in the as-prepared Ni_5Zn_{21} nanowires again. In other words, it is these Ni-rich microzones that are the origin of the low-temperature ferromagnetism of Ni_5Zn_{21} nanowires.

Another interesting issue is the vortex magnetization of the as-prepared Ni_5Zn_{21} nanowires array. Generally, the magnetic vortex is closely related to the shape of the studied magnetic units. Vortex magnetization has been demonstrated to exist in the ferromagnetic micro- and nanodots, -disks, -rings, -ellipses, -cones, and -bars.[28−33] However, almost no reports are about the vortex magnetization of FM-NM alloy and their nanowires. The origin of the vortex in our Ni_5Zn_{21} nanowires is not well-known up to now, but we believe that it must be associated with the shape of Ni-rich microzones. Through mass investigations of related documents, it is found that the vortex magnetic hysteresis loops of Ni_5Zn_{21} nanowires shown in Figure 7d are very similar to those of electrodeposited Ni microbars reported in ref 33. Considering the similarities of the studied element (Ni) and preparation method (electrodeposition), it can be inferred that the shape of the Ni-rich microzones in Ni_5Zn_{21} nanowires is probably barlike or disklike. This is consistent with the assumption obtained from the analyses to ZFC/FC curves, which illustrates the Ni-rich microzones are the plates normal to the long axis of nanowires. In Figure 7c,d, we also marked the nucleation (H_n) and annihilation (H_a) field of the vortex. It

is found that the vortex state varies with the temperature. Further study on the vortex magnetization may need much more experiments and micromagnetic simulations, and it is beyond the discussions in this paper.

The magnetic transport property of the Ni_5Zn_{21} nanowire array was measured at 5 K. The measurement was carried out with a modified four-electrode configuration also used by other authors (see Supporting Information).[34,35] With this configuration, the total resistance follows such a relation:

$$\frac{1}{R_{\text{total}}} = \frac{1}{R_{\text{NWs}}} + \frac{1}{R_{\text{PAA}}} \quad (1)$$

where R_{NWs} represents the total resistance of all conductive nanowires, and R_{PAA} stands for the resistance of the PAA template. Because the resistivity of alumina is far beyond that of metals and alloys, that is, $1/R_{\text{PAA}} \approx 0$, this will give rise to the relation $R_{\text{total}} \approx R_{\text{NWs}}$. Therefore, it can be considered that the measured total resistance is the resistance of the nanowire array. According to the measured resistance value, we also estimate that the number of conductive nanowires is about 4200 (taking the resistivity of nanowires as $\rho_{\text{zinc}} = 5.92 \times 10^{-8}$ Ω· m, the length as $L = 40$ μm, and the diameter as $d = 60$ nm). Hence, the measured magnetoresistance (MR) effect will be the collective behavior of this parallel nanowires assembly. Here, the MR is defined by the following equation:

$$\text{MR (\%)} = 100 \times \text{DR}/R_0 = 100 \times (R_{\text{H}} - R_0)/R_0 \quad (2)$$

where R_{H} and R_0 are the resistances with and without the magnetic field, respectively.

It can be seen from Figure 8a that the MR curve of the parallel configuration exhibits a broad peak, and the MR value is approximately 0.12%, while for the perpendicular configuration, the peak is narrower and the MR also has a slight improvement, amounting to about 0.18%. Although the MR values are small, it can be concluded that the MR is GMR instead of anisotropy MR (AMR). This is because AMR is associated with spin−orbit coupling and depends on the relative orientation of the field and the current in the samples. It is almost always positive for $\Delta R_{\parallel}$ (H || I) and negative for $\Delta R_{\perp}$ (H ⊥ I). [36] However, the MR values in our case are both negative, regardless of the field parallel or perpendicular to the current direction, which is the character of GMR.

The GMR effect in a granular system is usually related to spin-dependent scattering of conduction electrons at the interface between ferromagnetic granules and a nonmagnetic matrix, within ferromagnetic granules and spin−flip scattering from magnetic impurities. In as-prepared granular alloys, the magnetic moments of ferromagnetic granules are generally oriented randomly. When an external magnetic field is applied, these randomly oriented magnetic moments will be aligned and the resistance will drop. Theoretical investigations indicate that GMR depends on many factors, such as the size, shape, volume fraction, size distribution of magnetic granules, and the roughness between the granules and the matrix, etc.[37,38] It is also proposed that at low temperature the magnetoresistance mainly originates from the spin-dependent scattering occurring at the interface between magnetic granules and the matrix. So it can be expected that the GMR measured in our experiments also arises from the scattering of conduction electrons of the Ni_5Zn_{21} alloy at the interfaces between the Ni-rich microzones and the alloy matrix. The tiny GMR illustrates that the fraction of Ni-rich microzones is probably small. This is consistent with previous XRD and magnetic measurement results.

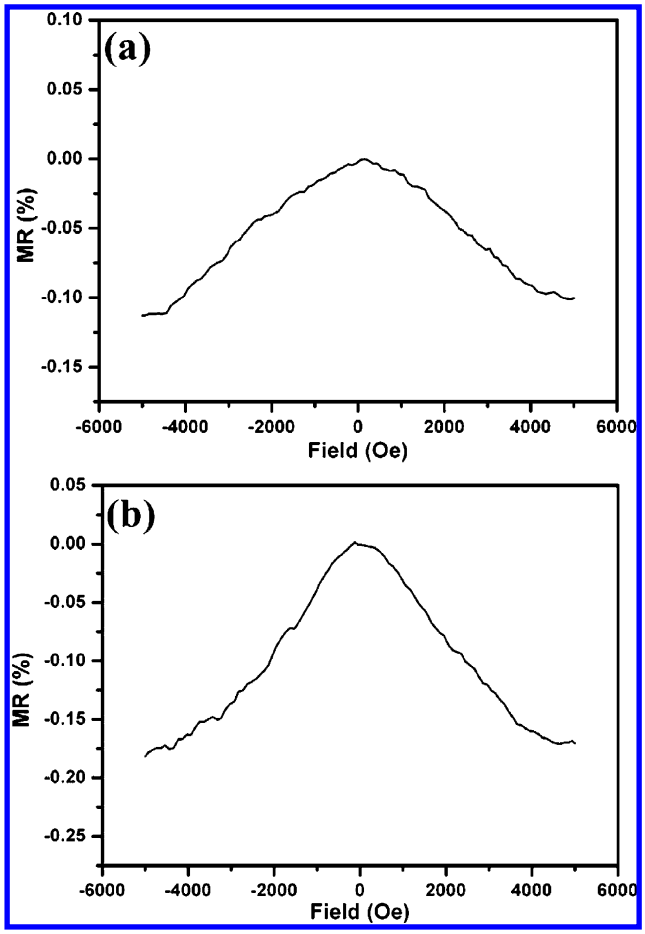

Figure 8. Magnetoresistance of as-deposited Ni_5Zn_{21} nanowire array measured at 5 K: (a) H || long axes of nanowires; (b) H ⊥ long axes of nanowires.

Another point that should be mentioned is that for the immiscible alloy, such as CoCu, the annealing usually can improve the GMR to some extent because it will have more Co clusters precipitated from the metastable CoCu alloy after annealing. However, for the NiZn alloy studied here, such phenomenon is not bound to take place, due to nickel and zinc being miscible. The detailed studies of the annealing effect on the structure, magnetic, and GMR properties are under investigation.

4. Conclusion

In summary, we have prepared Ni_5Zn_{21} alloy nanowires through template-assisted ECD method. The morphology and microstructures of these nanowires have been characterized in detail. Using EPMA, it is confirmed that there exist some Ni-rich microzones in the nanowires besides well-crystallized alloy crystallites. Subsequent magnetic measurements also confirm the existence of Ni-rich microzones. Moreover, the anisotropy of ZFC/FC curves as well as the vortex magnetization behavior suggest that the shape of Ni-rich microzones is probably barlike or disklike. The low-temperature magnetoresistive measurements of as-prepared nanowires show GMR behavior, and the tiny GMR values reflect the small number of Ni-rich microzones.

Finally, we would like to stress that our studies present detailed structural and physical property data on Zn-based FM-NM alloy nanowires, although the small GMR makes them hard to apply. Moreover, we observed the vortex magnetization behavior in FM-NM alloy nanowires for the first time. Such phenomenon enriches fundamental magnetics and may have potential applications in a magnetic bistable switch in the future.

Acknowledgment. The authors thank Mr. Weiwen Huang for his help in SQUID measurements and Mr. Shaokui Su for his assistance in magnetoresistance measurements. This work is supported by National Natural Science Foundation of China (Grant No. 10334060) and the "973" National Key Basic Research Program of China (Grant No. 2005 CB623602).

Supporting Information Available: Modified four-electrodes configuration. This material is available free of charge via the Internet at http://pubs.acs.org.

References and Notes

(1) Whitney, T. M.; Jiang, J. S.; Searson, P. C.; Chien, C. L. *Science* **1993**, *261*, 1316.

(2) Piraux, L.; George, J. M.; Despres, J. F.; Leroy, C.; Ferain, E.; Legras, R.; Ounadjela, K.; Fert, A. *Appl. Phys. Lett.* **1994**, *65*, 2484.

(3) Fert, A.; Piraux, L. *J. Magn. Magn. Mater.* **1999**, *200*, 338.

(4) Fedosyuk, V. M.; Schwarzacher, W.; Kasyutich, O. I.; Yi, G. *Phys. Low-Dimens. Struct.* **1999**, *12*, 61.

(5) Miyazaki, K.; Kainuma, S.; Hisatake, K.; Watanabe, T.; Fukumuro, N. *Electrochim. Acta* **1999**, *44*, 3713.

(6) Fedosyuk, V. M.; Kasyutich, O. I.; Schwarzacher, W. *J. Magn. Magn. Mater.* **1999**, *198*−*199*, 246.

(7) Blythe, H. J.; Fedosyuk, V. M.; Kasyutich, O. I.; Schwarzacher, W. *J. Magn. Magn. Mater.* **2000**, *208*, 251.

(8) Wang, Y. W.; Meng, G. W.; Liang, C. H.; Wang, G. Z.; Zhang, L. D. *Chem. Phys. Lett.* **2001**, *339*, 174.

(9) Wang, C. Z.; Meng, G. W.; Fang, Q. Q.; Peng, X. S.; Wang, Y. W.; Fang, Q.; Zhang, L. D. *Appl. Phys. A* **2002**, *35*, 738.

(10) Wang, Y. W.; Zhang, L. D.; Meng, G. W.; Peng, X. S.; Jin, Y. X.; Zhang, J. *J. Phys. Chem. B* **2002**, *106*, 2502.

(11) Zhang, Z. T.; Blom, D. A.; Gai, Z.; Thompson, J. R.; Shen, J.; Dai, S. *J. Am. Chem. Soc.* **2003**, *125*, 7528.

(12) Chu, S. Z.; Inoue, S.; Wada, K.; Kurashima, K. *Electrochim. Acta* **2005**, *51*, 820.

(13) Berkowitz, A. E.; Young, A. P.; Mitchell, J. R.; Zhang, S.; Carey, M. J.; Spada, F. E.; Parker, F. T.; Hutten, A.; Thomas, G. *Phys. Rev. Lett.* **1992**, *68*, 3745.

(14) Xiao, J. Q.; Jiang, J. S.; Chien, C. L. *Phys. Rev. Lett.* **1992**, *68*, 3749.

(15) Jia, C.; Liu, W. F.; Zhang, B.; Jin, C. G.; Yao, L. Z.; Cai, W. P.; Li, X. G. *Chem. Lett.* **2005**, *34*, 20.

(16) Liu, L. F.; Xie, S. S.; Song, L.; Gao, Y.; Liu, D. F.; Dou, X. Y.; Luo, S. D.; Wang, J. X.; Zhao, X. W.; Zhang, Z. X.; Xiang, Y. J.; Zhou, W. Y.; Wang, C. Y.; Wang, G. *Nanotechnology* **2006**, *17*, 19.

(17) Masuda, H.; Satoh, M. *Jpn. J. Appl. Phys.* **1996**, *35*, L126.

(18) Bories, C.; Bonino, J. P.; Rousset, A. *J. Appl. Electrochem.* **1999**, *29*, 1045.

(19) Bruet-Hotellaz, Bonino, J. P.; Rousset, A.; Marolleau; Chauveau, E. *J. Mater. Sci.* **1999**, *34*, 881.

(20) Mizutani, U. *Introduction to the Electron Theory of Metals*; Cambridge University Press: Cambridge, U.K., 2001.

(21) Cohen-Hyams, T.; Plitzko, J. M.; Hetherington, C. J. D.; Hutchison, J. L.; Yahalom, J.; Kaplan, W. D. *J. Mater. Sci.* **2004**, *39*, 5701.

(22) Vejpravova, J.; Plocek, J.; Niznansky, D.; Hutlova, A.; Rehspringer, J. L.; Sechovsky, V. *IEEE. Trans. Magn.* **2005**, *41*, 3469.

(23) Yu, R. H.; Zhang, X. X.; Tejada, J.; Zhu, J. *Phys. Rev. B* **1995**, *52*, R6987.

(24) Rhie, K.; Naugle, D. G.; O, B-H; Markert, J. T.; Morrish, A. H.; Zhou, X. Z. *J. Phys.: Condens. Matter.* **1995**, *7*, 3315.

(25) Kittel, C. *Introduction to Solid State Physics*, 7th ed.; John Wiley& Sons: New York, 1996.

(26) Mott, N. F.; Jones, H. *The Theory of the Properties of Metal and Alloys*; Oxford University Press: Oxford, U.K., 1932.

(27) Wheeler, M. A. *Phys. Rev.* **1939**, *56*, 1137.

(28) Zhu, X. B.; Grutter, P.; Metlushko, V.; Ilic, B. *Appl. Phys. Lett.* **2002**, *80*, 4789.

(29) Guslienko, K. Y.; Novosad, V.; Otani, Y.; Shima, H.; Fukamichi, K. *Appl. Phys. Lett.* **2001**, *78*, 3848.

(30) Zhu, F. Q.; Chern, G. W.; Tchernyshyov, O.; Zhu, X. C.; Zhu, J. G.; Chien, C. L. *Phys. Rev. Lett.* **2006**, *96*, 027205.

(31) Vavassori, P.; Zaluzec, N.; Metlushko, V.; Novosad, V.; Ilic, B.; Grimsditch, M. *Phys. Rev. B* **2004**, *69*, 214404.

(32) Hwang, M.; Redjdal, M.; Humphrey, F. B.; Ross, C. A. *J. Appl. Phys.* **2001**, *89*, 7582.

(33) Grujicic, D.; Pesic, B. *J. Magn. Magn. Mater.* **2005**, *288*, 196.

(34) Tian, M. L.; Kumar, N.; Xu, S. Y.; Wang, J. G.; Kurtz, J. S.; Chan, M. H. W. *Phys. Rev. Lett.* **2005**, *95*, 076802.

(35) Tian, M. L.; Wang, J. G.; Kurtz, J. S.; Liu, Y.; Chan, M. H. W.; Mayer, T. S.; Mallouk, T. E. *Nano Lett.* **2005**, *5*, 1247.

(36) Mendes, J. A.; Amaral, V. S.; Sousa, J. B.; Thomas, L.; Barbara, B. *J. Appl. Phys.* **1997**, *81*, 5208.

(37) Zhang, S. F.; Levy, P. M. *J. Appl. Phys.* **1993**, *73*, 5315.

(38) Zhang, S. F. *Appl. Phys. Lett.* **1992**, *61*, 1855.